APPLICATION OF CRAIG-BAMPTON REDUCTION TECHNIQUE AND 2D DYNAMIC INFINITE ELEMENT MODELING APPROACH TO MEMBRANE VIBRATION PROBLEMS

D. S. Liu **Y. W. Chen***

Department of Mechanical Engineering and Advanced Institute of Manufacturing with High-Tech Innovations
National Chung Cheng University
Chiayi, Taiwan

ABSTRACT

An approach is presented for solving membrane vibration problems using an integrated scheme consisting of the Craig-Bampton (CB) reduction technique and a 2D dynamic infinite element modeling (DIEM) method. In the proposed CB-DIEM scheme, the substructure domain is partitioned into multiple layers of geometrically-similar infinite elements (IEs) which use only the data of the boundary nodes. A convergence criterion based on the first invariant of the DIEM mass matrix is used to determine the optimal parameters of the CB-DIEM scheme, namely the proportionality ratio and number of layers in the DIEM partitioning process and the number of retained frequency modes in the CB reduction method. Furthermore, in implementing the CB method, the inversion of the global stiffness matrix is calculated using only the stiffness matrix of the first element layer. Having reduced the DIEM model, a coupled DIE-FE algorithm is employed to model the dynamic problems of the full structure, which removes the respective methods disadvantages while keeping their advantages. The validity and performance of the proposed CB-DIEM method are investigated by means of three illustrative problems.

Keywords: Craig-Bampton method, Dynamic infinite element model, Membrane vibration, Eigenvalue problem.

1. INTRODUCTION

The membrane structures have been discovered to be applicable in many fields, from micro-mechanical to architectural structures and aerospace craft [1-4]. Therefore, the estimation of the characteristics of the membrane is very important for the design of the structure. The finite element method is constantly adopted in such situations [5-7]. However, a large number of fine finite elements are required, cause the mesh modeling to be generally tedious and complex.

In the infinite element modeling (IEM) technique, the problem domain is discretized using a group of countable infinite elements (IEs) in such a way that each element layer is geometrically similar to all the layers above and below it in the partitioned structure. Thatcher [8, 9] combined the IEM method with a recurrence relation for the Laplace equation to solve problems with reentrant corners and unbounded domains. Ying [10] and Han [11] developed IEM formulations for the Laplace equation, plane elasticity problems, and corner problems, respectively. Go and Lin [12] and Go and Chen [13] integrated the IEM technique with a mesh generation scheme to solve various stress singularity problems. However, both studies considered only a small number of layers, and no guarantee was provided of numerical convergence. Ying [14] derived a transformation matrix describing the nodal displacement vector between the inner and outer layers of the degenerated IE structure, and showed that the existence of this matrix enabled the total stiffness matrix of the considered problem to be reduced to a combined stiffness matrix related only to the boundary nodes and their tractions. Notably, it was shown that the combined stiffness matrix had the form of a semi-positive definite matrix which converged to a certain constant quantity as the number of layers approached infinity.

The fractal finite element method (FFEM) also makes use of self-similar finite elements. Leung and Su [15-17] developed FFEM to model the crack region combined with a system stiffness matrix. Only a few degrees of freedom are required to model the singular behavior ahead of the crack tip. Reddy and Rao [18-20] used a FFEM to analyze cracks in a homogeneous, isotropic, and two-dimensional linear-elastic body subject to mixed-mode (modes I and II) loading conditions. However, some of these applications are limited to solving single crack problems with simplified load conditions.

* Corresponding author (ywc0314@gmail.com)

DOI : 10.1017/jmech.2018.45
Copyright © 2018 The Society of Theoretical and Applied Mechanics
https://doi.org/10.1017/jmech.2018.45 Published online by Cambridge University Press

Besides, some of the special element shapes are fixed to certain shape types (e.g. a round or rectangular shapes) that also prevent them from being easily combined with the existing FEM codes. Another attractive and powerful computational technique is to model the singularity region using the boundary element method (BEM) [21-25]. The BEM is based on an integral equation formulation and requires discretization of the problem boundary only. However, in the BEM, a re-modeling process is required to evaluate the effects on the response of changes in the properties of the singularity (e.g., the hole size, hole number, hole position, and so on). As a result, such methods, while highly accurate, are time consuming and inefficient.

Liu and Chiou [26, 27] proposed a hybrid IEM/FEM scheme for analyzing various types of elastic and singularity problems. Using this efficient numerical technique, a very fine mesh pattern can be established the singularities without increasing the degree of freedom of the global FEM solution. Moreover, it could be easily allowed to conduct parametric analyses for various crack sizes without changing the FE mesh. Liu, Chiou and Chen [28, 29] extended the IEM technique to elastostatic problems with heterogeneous material properties. Similarly, Liu *et al*. [30-32] extended the IEM formalism to the problem of moisture diffusion in 2D and 3D systems. Liu, Tu and Chung [33] examined the eigenvalue problem for microelectromechanical systems (MEMS) components and applied the displacement relationship between layers to solve the associated IEM formulation. In a later study, the same group [34] proposed a Plate IEM (PIEM) algorithm based on Mindlin-Reissner theory to investigate the effects of the hole size, hole position and hole profile/area on the bending strength of plates with through-thickness holes.

The Craig-Bampton method (CBM) is a well-known technique for reducing the size of finite element (FE) models; particularly when these models involve two or more connected subsystems. Liu and Lin [35] integrated CBM with a dynamic infinite element (DIE) formulation in order to improvement the efficiency of IEM without sacrificing its accuracy. The validity of the proposed approach was confirmed by comparing the results obtained for the vibration of a rectangular membrane with those obtained analytically and by FEM simulations, respectively.

Many studies have shown that the use of IEM to reduce the problem to one concerning the boundary nodes only yields a significant reduction in the computational cost. However, the accuracy of the solutions obtained for higher-order natural frequencies is rather poor. Liu and Lin [35] showed that this problem can be improved by integrating the dynamic IEM (DIEM) formulation with the CBM reduction technique. However, some related issues were not explored, such as the convergence of the element layers, the optimal number of retained frequency modes, and so on. Accordingly, this paper proposes a robust convergence criterion for the DIEM formulation based on the trace of the mass matrix. In addition, the efficiency of the CBM reduction process is improved by calculating the symmetric block- tridiagonal stiffness matrix using the method proposed by Jain *et al*. [36].

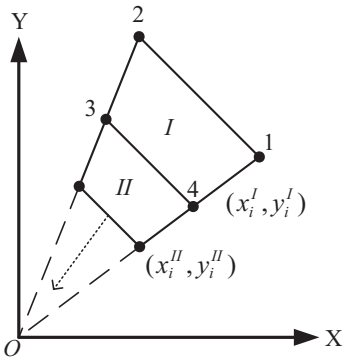


Fig. 1 Schematic representation of geometrically-similar 2D elements in IEM formulation.

2. 2D DYNAMIC INFINITE ELEMENT MODEL

2.1 Geometric Similarity of 2D Elements

The basic concept of IEM involves partitioning the computational domain into multiple layers of geometrically-similar elements. As shown in Fig. 1, for element *I* in the upper-most layer, the local nodes *i* are numbered 1, 2, 3, and 4, respectively, in the counterclockwise direction. Furthermore, for each node *i,* the global coordinates are denoted as (x_i^I, y_i^I). Taking the global origin *O* as the center of similarity, element *II* in the second layer can be obtained using a simple proportionality ratio *c*. More particularly, the global coordinates of elements *I* and *II* are related as follows:

$$\left(x_i^{II}, y_i^{II}\right) = \left(cx_i^I, cy_i^I\right) \tag{1}$$

where *c* is a proportionality ratio, As shown in Eq. (2), the coordinates of any point within element *I* can be expressed in terms of the nodal coordinates by means of a shape function ϕ_i.

$$\begin{cases} x^I = \sum_{i=1}^{4} \phi_i x_i^I \\ y^I = \sum_{i=1}^{4} \phi_i y_i^I \end{cases} \tag{2}$$

Multiplying both sides of Eq. (2) by the proportionality ratio *c*, the coordinates of the corresponding point in element *II* can then be obtained as:

$$\begin{cases} x^{II} = \sum \phi_i x_i^{II} = cx^I \\ y^{II} = \sum \phi_i y_i^{II} = cy^I \end{cases} \tag{3}$$

From Eq. (3), it is seen that quadrilateral elements *I* and *II* can both be mapped using the same square-shaped master element (where this element is defined in natural coordinates). In other words, if the coordinate node values of an element are similar to those of other elements, these elements are designated as similar elements.

https://doi.org/10.1017/jmech.2018.45 Published online by Cambridge University Press

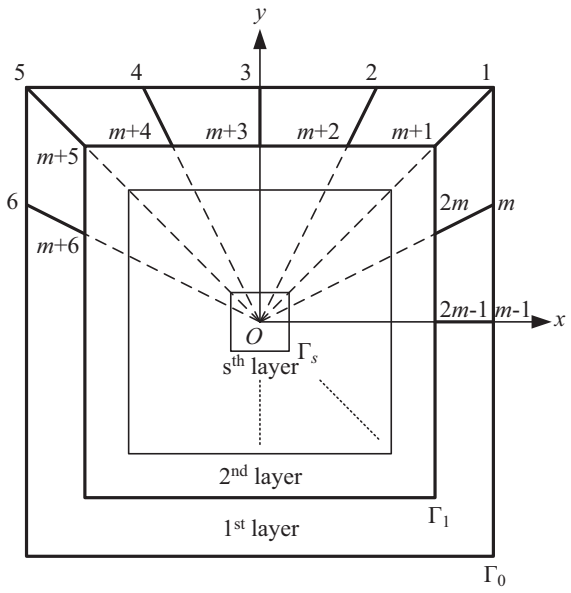


Fig. 2 IEM scheme around reference point O.

2.2 2D DIEM Formulation

This section derives the general 2D DIEM formulation for membrane vibration problems. The partitioning concept described in Section 2.1 can be illustrated schematically as shown in Fig. 2.

In meshing the computational domain, the outer boundary, Γ_0, is first discretized using a total of m master nodes, ordered in a counterclockwise direction. By choosing a similarity-partitioning point O and a proportionality ratio c, similar boundaries Γ_1, Γ_2, …, Γ_s, … of Γ_0 are then constructed with centers O and proportionality ratios c^1, c^2, …, c^s, …, respectively. For convenience, the region bounded by Γ_{i-1} and Γ_i is referred to hereafter as the ith element layer (i = 1, 2, …, s), where s is the total number of chosen layers. Having constructed the element layers, each boundary curve Γ_i is regularly discretized using the same number of nodes as that used for Γ_0. For each boundary curve, the nodal coordinates are determined directly from those of the master nodes with geometrically similar conditions. Finally, each element-layer is auto-meshed into m four-node quadrilateral elements, where these elements are similar to one another from the element-layers in a radial direction.

In general, the governing equation for the vibration of a membrane has the form shown in Eq. (4), where T is the tension force per unit length of the membrane edge and ρ is the mass density of the membrane and is a constant.

$$-T\left(\frac{\partial^2 W}{\partial x^2}+\frac{\partial^2 W}{\partial y^2}\right)=\rho h\frac{\partial^2 W}{\partial t^2} \tag{4}$$

By mapping from the physical coordinates to the natural coordinates, the unit element matrix equation for the vibration of the membrane can be obtained from Eq. (4) using Galerkin's weighted residual approach with the form:

$$[M]\{\ddot{u}\}+[K]\{u\}=0 \tag{5}$$

For a 2D elastic problem, the element mass and stiffness matrices are given respectively as:

$$\begin{cases}\left[M^e\right]=\rho h\left\{\int_D \phi_i\phi_j \det[J]\,d\zeta\,d\eta\right\}\\ \left[K^e\right]=T\left\{\int_D \frac{\partial\phi_i}{\partial\zeta}\frac{\partial\phi_j}{\partial\zeta}\det[J]\,d\zeta\,d\eta+\int_D \frac{\partial\phi_i}{\partial\eta}\frac{\partial\phi_j}{\partial\eta}\det[J]\,d\zeta\,d\eta\right\}\end{cases} \tag{6}$$

where

$$[J]=\begin{bmatrix}\frac{\partial x}{\partial\zeta} & \frac{\partial y}{\partial\zeta}\\ \frac{\partial x}{\partial\eta} & \frac{\partial y}{\partial\eta}\end{bmatrix}=\begin{bmatrix}\cdot & \cdot\\ \frac{\partial\phi_i}{\partial\zeta} & \cdot\\ \frac{\partial\phi_i}{\partial\eta} & \cdot\\ \cdot & \cdot\end{bmatrix}\begin{bmatrix}\cdot & \cdot\\ \cdot & \cdot\\ x_i & y_i\\ \cdot & \cdot\\ \cdot & \cdot\end{bmatrix} \tag{7}$$

is the Jacobian matrix, and (ζ, η) is represented as natural coordinates.

Recalling Eq. (1), and from Eq. (7), the determinants of the Jacobian matrices of the 1st and 2nd element layers, respectively, are related as follows:

$$\det[J]^{II}=c^2\det[J]^{I} \tag{8}$$

Therefore, the element matrices of the 1st and 2nd element layers are related as shown in Eq. (9), where the mass matrix $[M]$ and stiffness matrix $[K]$ of the 1st element layer have the forms shown in Eq. (10). Note that the mass matrix is simplified as a diagonal matrix by a lumped-mass formulation. Lumped-mass is preferred for computational speed in dynamic analysis.

$$\begin{cases}[M]^{II}=c^2[M]^{I}\\ [K]^{II}=[K]^{I}\end{cases} \tag{9}$$

$$\begin{cases}[M]^{I}=\begin{bmatrix}M_a & -D^T\\ -D & M_b\end{bmatrix}=\begin{bmatrix}L_a & 0\\ 0 & L_b\end{bmatrix}\\ [K]^{I}=\begin{bmatrix}K_a & -A^T\\ -A & K_b\end{bmatrix}\end{cases} \tag{10}$$

Recalling Eq. (5), the eigenvalue formulation of the first element layer in the DIEM can be defined as

$$\left\{[K]^{I}-\omega^2[M]^{I}\right\}\{u\}^{I}=0 \tag{11}$$

where $\{u\}^I=\{\delta_0\ \delta_1\}^T$, in which δ_0 denotes the nodal displacements of the outermost element layer in the DIEM. Equation (11) can be rewritten in matrix form as:

$$\left\{\begin{bmatrix}K_a & -A^T\\ -A & K_b\end{bmatrix}-\omega^2\begin{bmatrix}L_a & 0\\ 0 & L_b\end{bmatrix}\right\}\begin{Bmatrix}\delta_0\\ \delta_1\end{Bmatrix}=0 \tag{12}$$

https://doi.org/10.1017/jmech.2018.45 Published online by Cambridge University Press

According to the similarity principle described above, and the subsequent regular meshing rule, the mass and stiffness matrices of the s element layers can be expressed as the following set of algebraic equations:

$$\left\{\begin{bmatrix} K_a & -A^T \\ -A & K_b \end{bmatrix} - \omega^2 \begin{bmatrix} L_a & 0 \\ 0 & L_b \end{bmatrix}\right\}\begin{Bmatrix} \delta_0 \\ \delta_1 \end{Bmatrix} = 0$$

for 1st element-layer (13)

$$\left\{\begin{bmatrix} K_a & -A^T \\ -A & K_b \end{bmatrix} - \omega^2 c^2 \begin{bmatrix} L_a & 0 \\ 0 & L_b \end{bmatrix}\right\}\begin{Bmatrix} \delta_1 \\ \delta_2 \end{Bmatrix} = 0$$

for 2nd element-layer (14)

$$\left\{\begin{bmatrix} K_a & -A^T \\ -A & K_b \end{bmatrix} - \omega^2 c^{2(s-1)} \begin{bmatrix} L_a & 0 \\ 0 & L_b \end{bmatrix}\right\}\begin{Bmatrix} \delta_{s-1} \\ \delta_s \end{Bmatrix} = 0$$

for sth element-layer (15)

By expanding and arranging the equations for all the layers, adding the second equation for the i^{th} element-layer and the first equation for the $(i+1)^{th}$ element-layer, and letting $Q = K_b + K_a$ and $R = L_a + c^2 L_a$, the following formulations are obtained:

$$\left\{K_a\delta_0 - A^T\delta_1\right\} - \omega^2\left\{L_a\delta_0\right\} = 0 \tag{16}$$

$$\left\{-A\delta_0 + Q\delta_1 - A^T\delta_2\right\} - \omega^2\left\{R\delta_1\right\} = 0 \tag{17}$$

$$\left\{-A\delta_{i-1} + Q\delta_i - A^T\delta_{i+1}\right\} - \omega^2 c^{2(i-1)}\left\{R\delta_i\right\} = 0 \tag{18}$$

$$\left\{-A\delta_{s-2} + Q\delta_{s-1} - A^T\delta_s\right\} - \omega^2 c^{2(s-2)}\left\{R\delta_{s-1}\right\} = 0 \tag{19}$$

$$\left\{-A\delta_{s-1} + K_b\delta_s\right\} - \omega^2 c^{2(s-1)}\left\{L_b\delta_s\right\} = 0 \tag{20}$$

The eigenvalue formulation of the DIEM can be obtained by assembling the aforementioned equations follows:

$$\left(\left[K\right]_{IEM} - \omega^2\left[M\right]_{IEM}\right)\left\{u\right\}_{IEM} = 0 \tag{21}$$

where

$$\left[K\right]_{IEM} = \begin{bmatrix} K_a & -A & 0 & 0 & 0 & 0 \\ -A^T & Q & -A & 0 & 0 & 0 \\ 0 & -A^T & Q & -A & 0 & 0 \\ 0 & 0 & \ddots & \ddots & \ddots & 0 \\ 0 & 0 & 0 & -A^T & Q & -A \\ 0 & 0 & 0 & 0 & -A^T & K_b \end{bmatrix} \tag{22}$$

$$\left[M\right]_{IEM} = \begin{bmatrix} L_a & 0 & 0 & 0 & 0 & 0 \\ 0 & R & 0 & 0 & 0 & 0 \\ 0 & 0 & c^2R & 0 & 0 & 0 \\ 0 & 0 & 0 & \ddots & 0 & 0 \\ 0 & 0 & 0 & 0 & c^{2(s-2)}R & 0 \\ 0 & 0 & 0 & 0 & 0 & c^{2(s-1)}L_b \end{bmatrix} \tag{23}$$

$$\left\{u\right\}_{IEM} = \left\{\delta_0 \quad \delta_1 \quad \delta_2 \quad \cdots \quad \cdots \quad \delta_{s-1} \quad \delta_s\right\}^T \tag{24}$$

Before applying Eq. (21) for further numerical analysis, a detailed convergence study involving the DIEM mass matrix, $[M]_{IEM}$, must first be performed. In practice, the convergence (or otherwise) of the mass matrix depends primarily on the number of element layers selected in the DIEM formulation. Recalling Eq. (23), the trace of the DIEM mass matrix has the form:

$$Tr\left[M\right]_{IEM}^{(s)} = Tr\left(L_a + c^{2(s-1)}L_b + \sum_{n=2}^{s} c^{2(n-2)}R\right) \tag{25}$$

if $c < 1$, then

$$\lim_{s\to\infty} Tr\left[M\right]_{IEM}^{(s)} = Tr\left[M\right]_{IEM} \tag{26}$$

where s denotes the number of chosen element layers, and $Tr[M]_{IEM}$ converges to a certain constant quantity as the number of element layers approaches infinity. Notably, Eq. (25) shows that the convergence analysis involves only the mass matrix of the first element layer. In practice, Eq. (26) cannot be directly applied to the numerical DIEM formulation since the term "infinite" is not countable in a physical sense. However, if s is chosen as sufficiently large, the invariant of the mass matrix $\lim_{s\to\infty} Tr\left[M\right]_{IEM}^{(s)}$ approaches $Tr[M]_{IEM}$. The critical number of element-layers is determined when the desired accuracy criterion $\varepsilon = \left|Tr\left[M\right]_{IEM}^{(i+1)} - Tr\left[M\right]_{IEM}^{(i)}\right| \Big/ Tr\left|\left[M\right]_{IEM}^{(i+1)}\right| \times 100\% \le 10^{-3}$ is satisfied.

3. 2D DIEM REDUCTION USING CRAIG–BAMPTON METHOD

3.1 Reduction Procedure

The Craig-Bampton method (CBM) combines the motion of boundary points with modes of the subsystem under the assumption that the boundary points remain fixed. Using basic mass and stiffness matrices for the substructures, together with conditions of geometrical compatibility along the substructure boundaries, CBM employs two forms of generalized coordinates, namely "constraint modes" and "normal modes" to reduce the complexity of the IE model. The stiffness/mass matrix and displacement vector in the Eqs. (22)-(24) can be partitioned respectively as:

https://doi.org/10.1017/jmech.2018.45 Published online by Cambridge University Press

$$[K]_{IEM}=\begin{bmatrix} K^{BB} & K^{BI} \\ K^{IB} & K^{II} \end{bmatrix}=\left[\begin{array}{c|ccccc} K_a & -A & 0 & 0 & 0 & 0 \\ \hline -A^T & Q & -A & 0 & 0 & 0 \\ 0 & -A^T & Q & -A & 0 & 0 \\ 0 & 0 & \ddots & \ddots & \ddots & 0 \\ 0 & 0 & 0 & -A^T & Q & -A \\ 0 & 0 & 0 & 0 & -A^T & K_b \end{array}\right] \tag{27}$$

$$[M]_{IEM}=\begin{bmatrix} M^{BB} & 0 \\ 0 & M^{II} \end{bmatrix}=\left[\begin{array}{c|ccccc} L_a & 0 & 0 & 0 & 0 & 0 \\ \hline 0 & R & 0 & 0 & 0 & 0 \\ 0 & 0 & c^2R & 0 & 0 & 0 \\ 0 & 0 & 0 & \ddots & 0 & 0 \\ 0 & 0 & 0 & 0 & c^{2(s-2)}R & 0 \\ 0 & 0 & 0 & 0 & 0 & c^{2(s-1)}L_b \end{array}\right] \tag{28}$$

$$\{u\}_{IEM}=\begin{Bmatrix} u^B \\ u^I \end{Bmatrix}=\left\{\delta_0 \;\middle|\; \delta_1 \quad \delta_2 \quad \cdots \quad \cdots \quad \delta_{s-1} \quad \delta_s\right\}^T \tag{29}$$

where the superscripts B and I refer to boundary and interior nodes, respectively. The vectors u^B and u^I are physical displacements of boundary and interior points, respectively. According to the Craig-Bampton reduction method, the coordinate transformation equation relating the final coordinates of the substructure to the initial coordinates is given as:

$$\{u\}_{IEM}=\begin{Bmatrix} u^B \\ u^I \end{Bmatrix}=\begin{bmatrix} I & 0 \\ \phi^C & \phi^N \end{bmatrix}\begin{Bmatrix} p^B \\ p^N \end{Bmatrix}=[\phi]\{p\}_{IEM}, \quad p^B \equiv u^B \tag{30}$$

where matrices $[\phi^C]$ and $[\phi^N]$ are the desired matrices of the constraint modes and normal modes, respectively.

The constraint modes are defined as the mode shapes of the interior freedoms due to successive unit displacements of the boundary points, with all other boundary points being totally constrained. To determine the constraint modes, the forces acting at all the interior freedoms are set equal to zero, i.e.,

$$\left[K^{IB}\right]\left\{u^B\right\}+\left[K^{II}\right]\left\{u^I\right\}=\{0\} \tag{31}$$

or

$$\left\{u^I\right\}=-\left[K^{II}\right]^{-1}\left[K^{IB}\right]\left\{u^B\right\}\equiv\left[\phi^C\right]\left\{u^B\right\} \tag{32}$$

The normal modes are defined as the normal modes of the substructure given a totally constrained boundary. In other words, they represent the eigenvectors of the eigenvalue problem:

$$\left\{u^I\right\}=\left\{\phi^I\right\}e^{i\omega t}, \quad \left([I]-\omega^2\left[K^{II}\right]^{-1}\left[M^{II}\right]\right)\left\{\phi^I\right\}=0 \tag{33}$$

These eigenvectors form the respective columns of matrix $[\phi^N]$.

As can be seen from Eq. (27), the $[K^{II}]$ is a symmetric block-tridiagonal matrix. Consequently, the inversion of $[K^{II}]$, i.e., $[K^{II}]^{-1}$, can be written as the following a semi-separable matrix:

$$\left[K^{II}\right]^{-1}=\begin{bmatrix} U_1V_1^T & U_1V_2^T & U_1V_3^T & \cdots & U_1V_s^T \\ V_2U_1^T & U_2V_2^T & U_2V_3^T & \cdots & U_2V_s^T \\ V_3U_1^T & V_3U_2^T & U_3V_3^T & \cdots & U_3V_s^T \\ \vdots & \vdots & \vdots & \ddots & \vdots \\ V_sU_1^T & V_sU_2^T & V_sU_3^T & \cdots & U_sV_s^T \end{bmatrix} \tag{34}$$

where matrices $[U_i]$ and $[V_i]$ are computed as:

$$\begin{aligned} &U_1=I \\ &U_2=A^{-1}Q \\ &U_{i+1}=A^{-1}\left(QU_i-A^TU_{i-1}\right), \quad i=2,\ldots,s-1 \\ &V_s^T=\left(K_bU_s-A^TU_{s-1}\right)^{-1} \\ &V_{s-1}^T=V_s^TQA^{-1} \\ &V_i^T=\left(V_{i+1}^TQ-V_{i+2}^TA^T\right)A^{-1}, \quad i=s-2,\ldots,1 \end{aligned} \tag{35}$$

According to Jain *et al*. [36], the diagonal blocks of $[K^{II}]^{-1}$, denoted as D_i, can be obtained recursively as:

$$\begin{aligned} &D_1=\left(Q-AS_1^T\right)^{-1} \\ &D_i=\left(Q-AS_i^T\right)^{-1}\left(I+A^TD_{i-1}S_{i-1}\right), \quad i=2,\ldots,s-1 \\ &D_s=K_b^{-1}\left(I+A^TD_{s-1}S_{s-1}\right) \end{aligned} \tag{36}$$

where matrices $[S_i]$ are defined as follows:

$$V_{i+1}^T=V_i^TS_i \tag{37}$$

In the present study, $[S_i]$ are computed using the following numerically stable recursive procedure:

$$\begin{aligned} &S_2=AK_b^{-1} \\ &S_i=A\left(Q-S_{i+1}A^T\right)^{-1}, \quad i=s-2,\ldots,1 \end{aligned} \tag{38}$$

The remaining block entries are then computed in a numerically stable manner as follows:

$$\left[K^{II}\right]^{-1}=\begin{bmatrix} D_1 & D_1S_1 & D_1S_1S_2 & \cdots D_1S_1\ldots S_{s-1} \\ (D_1S_1)^T & D_2 & D_2S_2 & \cdots D_2S_2\ldots S_{s-1} \\ (D_1S_1S_2)^T & (D_2S_2)^T & D_3 & \cdots D_3S_3\ldots S_{s-1} \\ \vdots & \vdots & \vdots & \ddots \quad \vdots \\ (D_1S_1\ldots S_{s-1})^T & (D_2S_2\ldots S_{s-1})^T & (D_3S_3\ldots S_{s-1})^T & \cdots \quad D_s \end{bmatrix} \tag{39}$$

https://doi.org/10.1017/jmech.2018.45 Published online by Cambridge University Press

As can be seen from the aforementioned equations, $[K^{II}]^{-1}$ is calculated using only the stiffness matrix of the first element layer, that is greatly improved the efficiency of computational work.

Finally, the eigenvalue formulation of the CB-DIEM scheme can be obtained by substituting the coordinate transformation relation, i.e., Eq. (30), into Eq. (21) and then pre-multiplying by the transpose of $[\phi]$, i.e.,

$$\left([\phi]^T [K]_{IEM} [\phi] - \omega^2 [\phi]^T [M]_{IEM} [\phi]\right)\{p\}_{IEM} = 0 \quad (40)$$

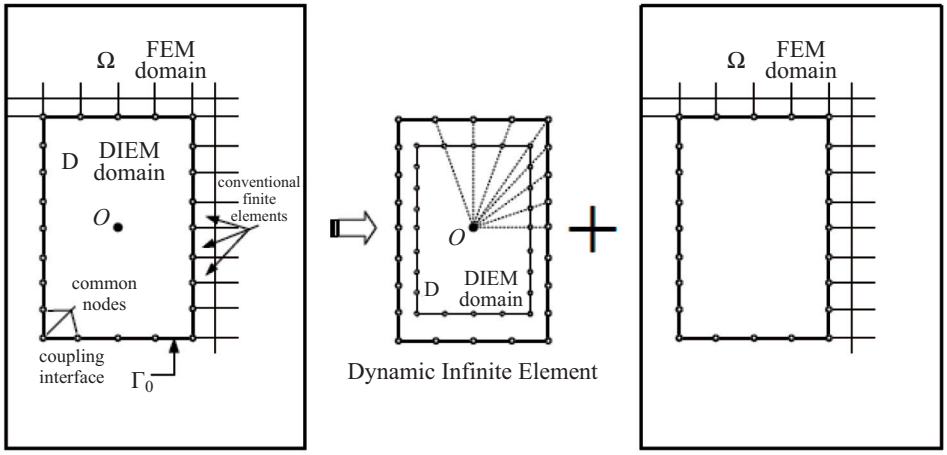


Fig. 3 Schematic diagram of DIE-FE coupling method.

3.2 Solution of Membrane Vibration Problems Using Coupled CB-DIEM and FEM Scheme

As described in Sections 2 and 3, in the CB-DIEM scheme, the problem domain is degenerated into a cascaded series of layer-wise elements with similar shapes, and the numerous resultant DOFs are then condensed using the Craig-Bampton reduction method. The membrane vibration problems considered in the present study are solved by means of FEM simulations. Thus, the nodes on the outer boundary of the DIEs are taken as interface common nodes between the DIE and FE subdomains. Importantly, since each DIE-reduced mass/stiffness matrix is pre-determined, the elements can be treated as regular FEs, and their DIE-reduced mass/stiffness matrices assembled into a global combined mass/stiffness matrix. Figure 3 illustrates the assembling scheme of DIE-FE coupling method.

As shown, the two domains, namely D and Ω (modeled using DIEs and FEs, respectively) are joined by a coupling interface, Γ_0. In the conventional FEM scheme, the algebraic-assembled element equations are derived from Eq. (5) in the form of

$$\left([K]_{FEM} - \omega^2 [M]_{FEM}\right)\{u\}_{FEM} = 0 \quad (41)$$

The global eigenvalue formulation can be expressed by assembling Eqs. (21) and (41) as follows:

$$\left(\begin{bmatrix} K_{FEM^*} & 0 & 0 \\ 0 & K_{couple} & 0 \\ 0 & 0 & K_{IEM^*} \end{bmatrix} - \omega^2 \begin{bmatrix} M_{FEM^*} & 0 & 0 \\ 0 & M_{couple} & 0 \\ 0 & 0 & M_{IEM^*} \end{bmatrix}\right)\begin{Bmatrix} u_{FEM^*} \\ u_{couple} \\ u_{IEM^*} \end{Bmatrix} = 0 \quad (42)$$

or

$$\left([K]_{global} - \omega^2 [M]_{global}\right)\{u\}_{global} = 0, \quad (43)$$

where

$$[K]_{global} = \begin{bmatrix} K_{FEM^*} & 0 & 0 \\ 0 & K_{couple} & 0 \\ 0 & 0 & K_{IEM^*} \end{bmatrix},$$

$$[M]_{global} = \begin{bmatrix} M_{FEM^*} & 0 & 0 \\ 0 & M_{couple} & 0 \\ 0 & 0 & M_{IEM^*} \end{bmatrix},$$

$$\{u\}_{global} = \begin{Bmatrix} u_{FEM^*} \\ u_{couple} \\ u_{IEM^*} \end{Bmatrix} \quad (44)$$

where the subscripts FEM^* and IEM^* are the FEM and IEM domain except coupled nodes, respectively. According to Eq. (30), the coordinate transformation equation relating the final coordinates, p, to the initial coordinates, u, is given by

Finally, the global eigenvalue formulation can be obtained by substituting the coordinate transformation relation, Eq. (45), into Eq. (43) and then pre-multiplying by the transpose of $[\alpha]$ to give

$$\left([\alpha]^T [K]_{global} [\alpha] - \omega^2 [\alpha]^T [M]_{global} [\alpha]\right)\{p\}_{global} = 0 \quad (46)$$

https://doi.org/10.1017/jmech.2018.45 Published online by Cambridge University Press

or

$$\left(\left[\bar{K}\right]_{global}-\omega^2\left[\bar{M}\right]_{global}\right)\{p\}_{global}=0,$$

$$\left[\bar{K}\right]_{global}=[\alpha]^T\left[K\right]_{global}[\alpha],$$

$$\left[\bar{M}\right]_{global}=[\alpha]^T\left[M\right]_{global}[\alpha] \quad (47)$$

where $\left[\bar{M}\right]_{global}$ and $\left[\bar{K}\right]_{global}$ are the reduced mass and stiffness matrices, respectively.

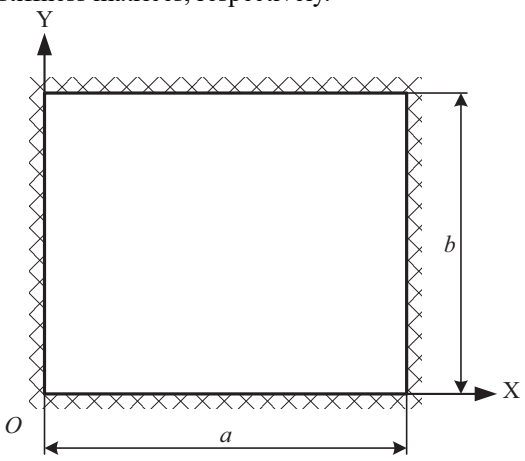


Fig. 4 Schematic illustration of rectangular membrane clamped at all four edges.

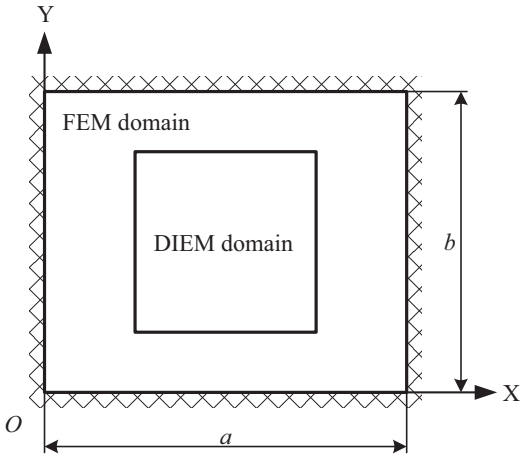


Fig. 5 DIE-FE coupling computational model of clamped rectangular membrane.

4. CASE STUDIES

4.1 Clamped Rectangular Membrane

Consider the clamped rectangular membrane shown in Fig. 4. Let the membrane dimensions and properties be defined as follows: a = 1.2 m, b = 1 m, thickness h = 25 × 10^{-6} m, tension force per unit edge length T = 3300 N/m, and mass density ρ = 2330 kg/m^3. Furthermore, assume that the membrane is rigidly clamped on all four sides. The DIE-FE coupling computational model is shown in Fig. 5. In implementing the DIE-FE model, 64 interface nodes are deployed at the coupled DIEM-FEM boundary and the FE subdomain is meshed using 224 four-node quadrilateral elements. Finally, the DIEM domain is located in the center of the rectangular membrane and has a square shape with a side length of 0.8 m. The mesh pattern is shown in Fig. 6.

For comparison purposes, the natural frequencies obtained by the CB-DIEM method for the six lowest

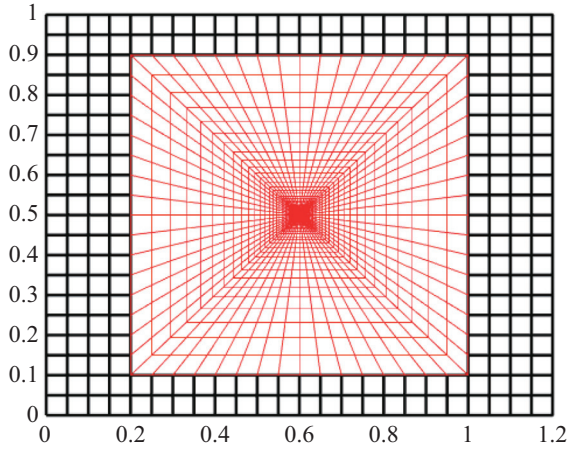


Fig. 6 Mesh configuration and node arrangement of coupled DIE-FE model of clamped rectangular membrane.

Table 1 Relationship between proportionality ratio, number of element layers and element aspect ratio for clamped membrane problem.

Proportionality Ratio c	Number of Element Layers s	Aspect Ratio of Element
0.8	26	1.6
0.825	29	1.4
0.85	34	1.2
0.875	40	1
0.9	49	1.25

modes are also estimated using linear transverse vibration theory. In other words, the eigenvalues $\beta_{m,n}$ and the natural frequency $\omega_{m,n}$ are estimated respectively as:

$$\beta_{m,n}=\sqrt{\left[\left(\frac{m}{a}\right)^2+\left(\frac{n}{b}\right)^2\right]},\quad m,\ n=1,\ 2,\ \ldots \quad (48)$$

$$\omega_{m,n}=\pi\sqrt{\left[\left(\frac{m}{a}\right)^2+\left(\frac{n}{b}\right)^2\right]\frac{T}{\rho h}},\quad m,\ n=1,\ 2,\ \ldots \quad (49)$$

As discussed in Section 2.2, the convergence of the CB-DIEM formulation depends on both the chosen number of element layers and the value assigned to the

https://doi.org/10.1017/jmech.2018.45 Published online by Cambridge University Press

proportionality ratio c. As shown in Table 1, the required number of element-layers increases with an increasing proportionality ratio. For example, given a proportionality ratio of c = 0.80, 26 element layers are required to obtain convergence. However, for a higher proportionality ratio of c = 0.90, the number of required element layers increases to 49. As a result, the choice of c is of critical importance in determining the convergence behavior and efficiency of the CB-DIEM scheme. For an ideal element, the aspect ratio should have a value of 1.0. From Table 1, an aspect ratio of 1.0 is obtained for a proportionality ratio equal to 0.875.

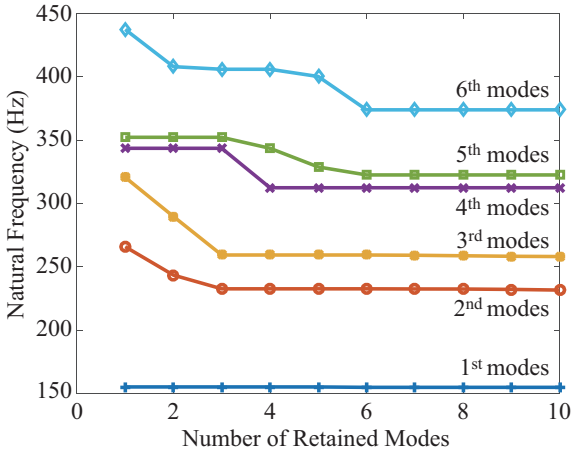


Fig. 7 Numerical solutions obtained from CB-DIEM scheme for first six natural frequencies of clamped membrane as function of number of retained modes in CBM.

Table 2 First six natural frequencies of clamped rectangular membrane. (Hz)

Methods	Mode No.					
	1	2	3	4	5	6
Abaqus	154.51	230.07	256.30	306.64	317.50	366.38
Error (%)	0.26	0.54	0.60	1.03	0.92	1.12
CB-DIEM	154.86	231.66	258.13	312.47	322.57	373.98
Error (%)	0.03	0.15	0.1	0.85	0.66	0.93
Exact	154.91	231.31	257.85	309.83	320.44	370.54

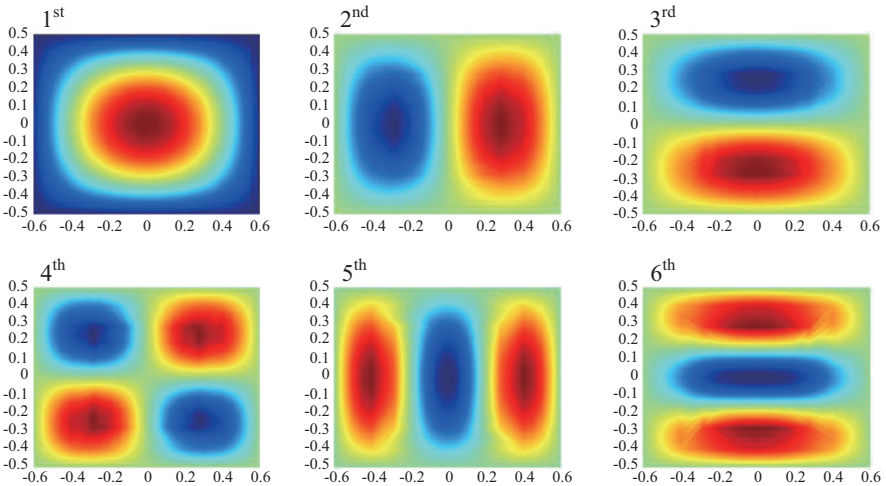


Fig. 8 First six mode shapes of clamped rectangular membrane.

Figure 7 shows the results obtained by the proposed CB-DIEM method for the first six natural frequencies of the clamped membrane given different numbers of retained modes in the CBM formalism. As shown, the convergence of the CB-DIEM method depends not only on the proportionality constant c and number of element layers s, but also on the number of retained modes. For example, in the present case, convergent solutions for the natural frequencies of the clamped membrane are obtained given a minimum of six retained modes; Therefore,

https://doi.org/10.1017/jmech.2018.45 Published online by Cambridge University Press

ten retained modes are selected to maintain a sufficiently conservative margin for following example problems.

Overall, the results presented above indicate that in solving the clamped membrane vibration problem, the proportionality ratio should be set as $c = 0.875$, the number of element layers as $s = 40$. Table 2 compares the results obtained from the CB-DIEM method for the first six natural frequencies of the clamped membrane with those obtained via Abaqus (480 elements, M3D4) simulations. It is observed that the CB-DIEM results are in good agreement with the theoretical results for all six natural frequencies. Figure 8 shows the CB-DIEM results for the first six mode shapes of the clamped rectangular membrane.

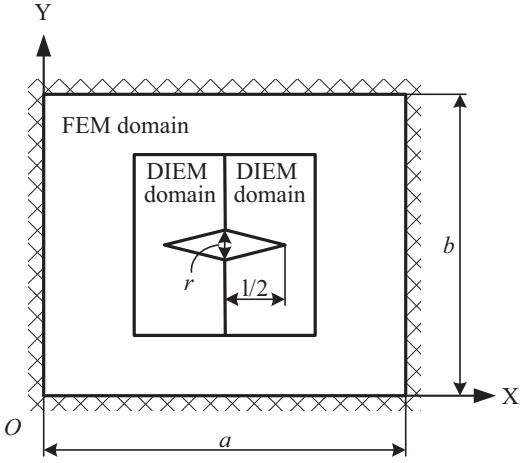


Fig. 9 Schematic illustration of center-cracked rectangular membrane clamped at all four edges.

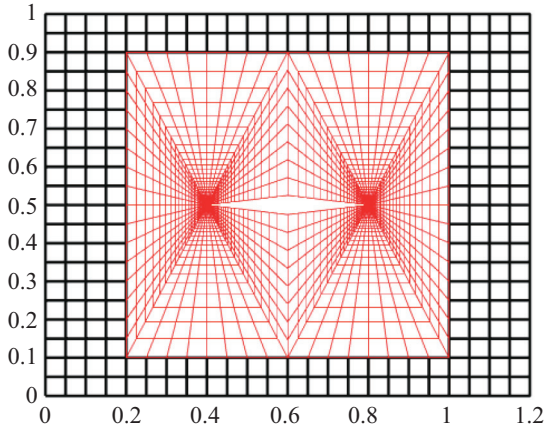


Fig. 10 Mesh configuration and node arrangement of DIE-FE model for clamped center-cracked rectangular membrane.

Table 3 First six natural frequencies of clamped rectangular membrane. (Hz)

Methods	Crack Length (m)	Mode No.					
		1	2	3	4	5	6
Abaqus	$l = 0$	154.51	230.07	256.30	306.64	317.50	366.38
	$l = 0.10$	154.53	230.05	254.61	306.64	317.52	366.41
	$l = 0.15$	154.54	230.22	251.12	306.84	317.70	366.47
	$l = 0.20$	154.54	230.04	246.33	306.47	317.54	366.44
	$l = 0.25$	154.52	230.12	239.40	306.17	317.33	363.19
	$l = 0.30$	154.55	230.03	231.80	305.49	317.55	358.56
CB-DIEM	$l = 0$	154.86	231.66	258.13	312.47	322.57	373.98
	$l = 0.10$	154.97	231.44	256.46	310.46	321.77	375.39
	$l = 0.15$	154.96	231.42	251.71	310.40	321.81	374.78
	$l = 0.20$	154.95	231.41	245.42	310.18	321.83	372.56
	$l = 0.25$	155.10	231.55	237.46	309.48	321.84	367.38
	$l = 0.30$	155.11	229.04	231.54	308.60	321.85	362.63

4.2 Clamped Rectangular Membrane with Center-Crack

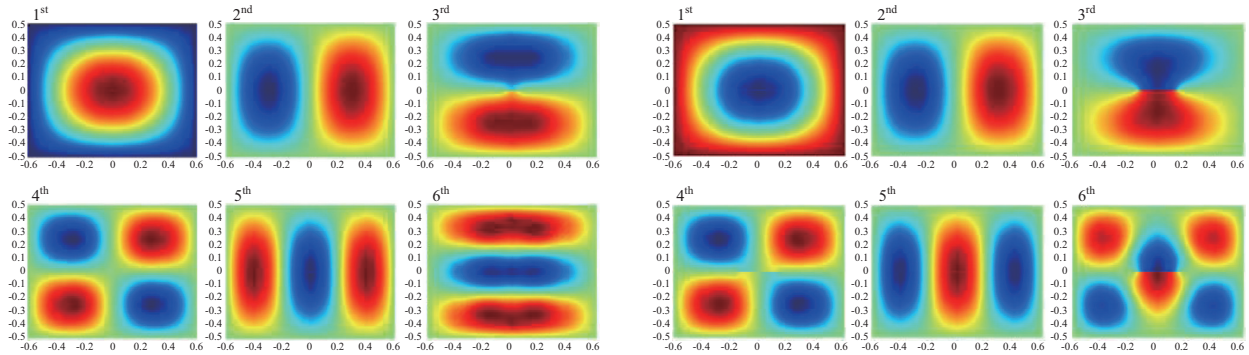
The second example considers a rectangular membrane containing a center through-thickness crack, as shown in Fig. 9. The dimensions and properties of the membrane are assigned as follows: $a = 1.2$ m, $b = 1$ m, thickness $h = 25 \times 10^{-6}$ m, tension force per unit edge length $T = 3300$ N/m, and mass density $\rho = 2330$ kg/m^3. It is assumed that the membrane is rigidly clamped on all four sides and the crack has a length l and width r. In implementing the CB-DIEM scheme, the crack width is assigned a constant value of $r = 0.0001$ m, while the crack length l is assigned various values in the range of $l = 0.1 \sim 0.3$ m. Figure 10 shows the mesh configuration and node arrangement of the DIE-FE model.

As in the previous example, the parameters of the CB-DIEM scheme are set as follows: proportionality ratio $c = 0.875$, number of element layers $s = 40$, and number of retained modes = 10. Table 3 compares the results obtained for the first six natural frequencies of the clamped membrane for various crack lengths l with those obtained from Abaqus simulations. For both solution methods, the third natural frequency of the membrane reduces with an increasing crack length. Figures 11(a)

https://doi.org/10.1017/jmech.2018.45 Published online by Cambridge University Press

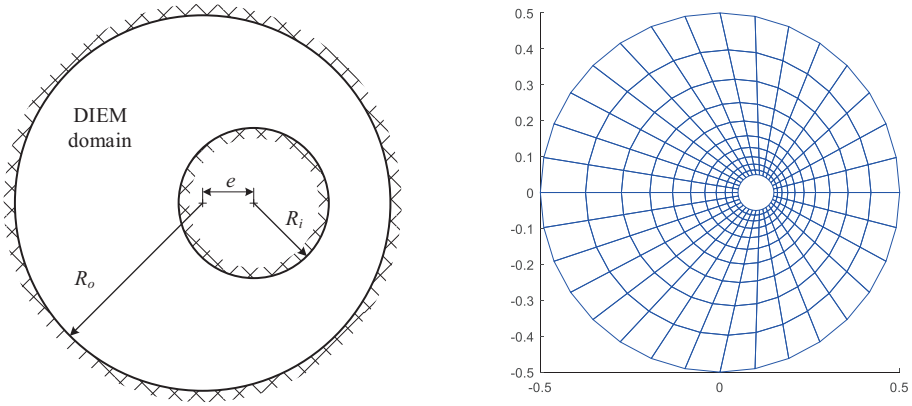
and 11(b) show the results obtained from the proposed CB-DIEM method for the first six mode shapes of the center-cracked rectangular membrane given crack lengths of l = 0.1 m and l = 0.3 m, respectively. As discussed above, the third vibration mode is highly sensitive to the crack length. It is observed in Fig. 11 that the sixth mode shape also changes as the crack length increases (as shown also in Table 3).

As a result, a good qualitative agreement is obtained between the two sets of results in every case. Furthermore, the results of CB-DIEM are obtained just need to adjust the reference point. Using these efficient numerical



(a) l = 0.1 m (b) l = 0.3 m

Fig. 11 First six mode shapes of clamped center-cracked rectangular membrane.



(a) Schematic illustration (b) Mesh configuration

Fig. 12 Schematic illustration and mesh configuration of clamped eccentric annular membrane.

techniques, a very fine mesh pattern can be stablished around each crack tip without increasing the degree of freedom of the global FEM solution. One is easily allowed to conduct parametric analyses for various crack sizes without changing the FE mesh.

4.3 Clamped Eccentric Annular Membrane

The third example considers the eccentric annular membrane shown in Fig. 12(a). The membrane is rigidly clamped at both the inner and outer boundaries with an eccentricity e, and the dimensions and properties of the membrane are set as follows: R_o = 0.5 m, R_i = 0.05 m, thickness h = 25 × 10^{-6} m, tension force per unit edge length T = 3300 N/m, and mass density ρ = 2330 kg/m^3. Figure 12(b) shows the mesh configuration and node arrangement of the corresponding CB-DIEM model. Note that the number of element layers s = 10. Furthermore, the proportionality ratio c is set as:

$$c = \left(\frac{R_o}{R_i} \right)^{\frac{1}{s}} \tag{50}$$

and the number of retained nodes in the CBM reduction procedure is set as 10.

Table 4 shows the solutions obtained for the first six natural frequencies of the clamped annular membrane, those solutions also obtained by Abaqus simulations. The eccentric hole is considered, the inner circle is shifted to the right 0.02 m ~ 0.1 m. As discussed above, the first vibration mode is highly sensitive to the eccentricity. Figures 13(a) and 13(b) show the results obtained from the proposed CB-DIEM method for the first six mode shapes of the clamped annular membrane without/with eccentricity, respectively.

This is another case to show the convenience of CB-DIEM. The results are obtained just need to adjust the coordinates of inner circle. The parametric analyses

https://doi.org/10.1017/jmech.2018.45 Published online by Cambridge University Press

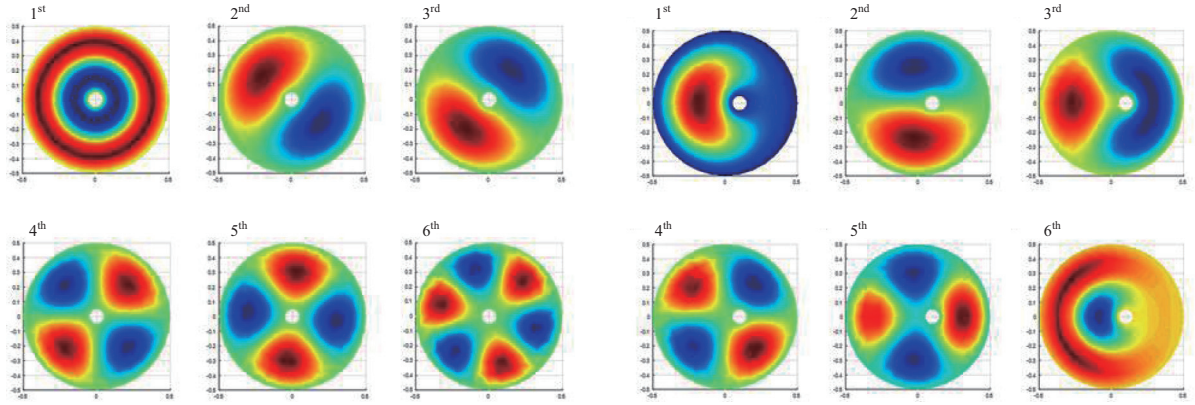
for various eccentricity are easy to be conducted using these numerical techniques.

5. CONCLUSIONS

This study has combined the Craig-Bampton (CB) reduction method with a dynamic infinite element modeling (DIEM) technique to examine the frequency response of clamped membrane structures. In implementing the proposed CB-DIEM model, the number of element layers, the proportionality ratio, and the number of retained modes have been determined using a convergence criterion based on the first invariant of the DIEM mass matrix and the assumption of an ideal element aspect ratio equal to 1. The convergence analysis involves only the mass matrix of the first element layer. Furthermore, the inversion of the symmetric block-tridiagonal global stiffness matrix has been computed using the method proposed by Jain *et al*. (2007) such that only the stiffness matrix of the first element layer need be considered.

Table 4 First six natural frequencies of clamped eccentric annular membrane. (Hz)

Methods	Eccentricity (m)	Mode No.					
		1	2	3	4	5	6
Abaqus	$e = 0$	250.06	295.9	295.98	381.68	381.85	465.86
	$e = 0.02$	249.04	295.79	297.24	381.83	381.90	465.84
	$e = 0.04$	246.48	295.81	301.16	382.24	382.36	465.65
	$e = 0.06$	242.65	295.23	306.63	382.62	382.84	468.24
	$e = 0.08$	238.33	294.56	313.11	383.51	384.14	465.23
	$e = 0.10$	234.05	294.40	319.77	384.62	387.12	460.03
CB-DIEM	$e = 0$	248.26	293.07	293.07	376.40	376.40	456.88
	$e = 0.02$	247.23	293.01	294.50	376.53	376.53	456.87
	$e = 0.04$	244.49	292.81	298.40	376.90	376.96	456.85
	$e = 0.06$	240.70	292.49	303.98	377.47	377.80	456.84
	$e = 0.08$	236.42	292.06	310.42	378.18	379.26	456.90
	$e = 0.10$	231.98	291.55	316.98	378.94	381.66	448.10



(a) $e = 0$ m (b) $e = 0.1$ m

Fig. 13 First six mode shapes of clamped eccentric annular membrane.

The validity of the proposed CB-DIEM method has been demonstrated by means of three illustrative examples involving a simple clamped rectangular membrane, a clamped rectangular membrane containing a through-thickness center crack, and a clamped annular membrane. In the first two examples, the solutions obtained for the first six natural frequencies of the membrane have been compared with those obtained via Abaqus simulations. In general, a good agreement has been observed between the various results. For the case of a membrane with a center crack, it has been shown that the third and sixth natural frequencies are particularly sensitive to the length of the center crack. For the clamped eccentric annular membrane, the CB-DIEM solutions have shown that the first natural frequency of the membrane reduces as the eccentricity increases.

In general, the results presented in this study have shown that the proposed CB-DIEM algorithm provides a fast, direct and accurate tool for simulating the dynamic characteristics of membrane structures. In particular, the first example has demonstrated the general feasibility and accuracy of the proposed method, while the second

https://doi.org/10.1017/jmech.2018.45 Published online by Cambridge University Press

example has demonstrated the applicability of the proposed method to geometric singularity problems (e.g., cracks). Finally, the third example has shown the feasibility for implementing the proposed scheme with a proportionality ratio greater than 1.0, and that is used in the vibration analysis of eccentric membrane structures.

ACKNOWLEDGEMENTS

This work was partially supported by the Advanced Institute of Manufacturing with High-tech Innovations (AIM-HI) from The Featured Areas Research Center Program within the framework of the Higher Education Sprout Project by the Ministry of Education (MOE) in Taiwan. This research was also supported by R.O.C. MOST Foundation Contract No. MOST107-3017-F-194 -001.

REFERENCES

1. Xu, R., Li, D. X., Jiang, J. P. and Liu, W., "Nonlinear Vibration Analysis of Membrane SAR Antenna Structure Adopting a Vector Form Intrinsic Finite Element," *Journal of Mechanics*, **31**, pp. 269-277 (2015).
2. Xu, R., Li, D. X., Jiang, J. P. and Liu, W., "Adaptive Fuzzy Vibration Control of Smart Structure with VFIFE Modeling," *Journal of Mechanics*, **31**, pp. 671-682 (2015).
3. João, L. S., Carvalho, R. and Fangueiro, R., "A Study on the Durability Properties of Textile Membranes for Architectural Purposes," *Procedia Engineering*, **155**, pp. 230-237 (2016).
4. Long, Z. *et al*., "Micro-Membrane Electrode Assembly Design to Precisely Measure the in Situ Activity of Oxygen Reduction Reaction Electrocatalysts for PEMFC," *Analytical Chemistry*, **89**, pp. 6309-6313 (2017).
5. Houmat, A., "A Sector Fourier P-Element for Free Vibration Analysis of Sectorial Membranes," *Computers & Structures*, **79**, pp. 1147-1152 (2001).
6. Houmat, A., "Free Vibration Analysis of Membranes Using the H-P Version of the Finite Element Method," *Journal of Sound and Vibration*, **282**, pp. 401-410 (2005).
7. Houmat, A., "Free Vibration Analysis of Arbitrarily Shaped Membranes Using the Trigonometric P-Version of the Finite-Element Method," *Thin-Walled Structures*, **44**, pp. 943-951 (2006).
8. Thatcher, R. W., "Singularities in the Solution of Laplace's Equation in Two Dimensions," *Journal of the Institute of Mathematics and Its Applications*, **16**, pp. 303-319 (1975).
9. Thatcher, R. W., "On the Finite Element Method for Unbounded Region," *SIAM Journal on Numerical Analysis*, **15**, pp. 466-477 (1978).
10. Ying, L. A., "The Infinite Similar Element Method for Calculating Stress Intensity Factors," *Scientia Sinica*, **21**, pp. 19-43 (1978).
11. Han, H. D. and Ying, L. A., "An Iterative Method in the Finite Element," *Mathematica Numerica Sinica*, **1**, pp. 91-99 (1979).
12. Go, C. G. and Lin, Y. S., "Infinitely Small Element for the Problem of Stress Singularity," *Computers & Structures*, **37**, pp. 547-551 (1991).
13. Go, C. G. and Chen, G. C., "On the Use of an Infinitely Small Element for the Three-Dimensional Problem of Stress Singularity," *Computers & Structures*, **45**, pp. 25-30 (1992).
14. Ying, L. A., "An Introduction to the Infinite Element Method," *Mathematics in Practice Theory*, **2**, pp. 69-78 (1992).
15. Leung, A. Y. T. and Su, R. K. L., "Mode I Crack Problems by Fractal Two Level Finite Element Methods," *Engineering Fracture Mechanics*, **48**, pp. 847-859 (1994).
16. Leung, A. Y. T. and Su, R. K. L., "Mixed-Mode Two-Dimensional Crack Problem by Fractal Two Level Finite Element Method," *Engineering Fracture Mechanics*, **51**, pp. 889-895 (1995).
17. Leung, A. Y. T. and Su, R. K. L., "Fractal Two-Level Finite Element Method for Cracked Kirchhoff's Plates using DKT Elements," *Engineering Fracture Mechanics*, **54**, pp. 703-711 (1996).
18. Reddy, R. M. and Rao, B. N., "Fractal Finite Element Method Based Shape Sensitivity Analysis of Mixed-mode Fracture," *Finite Elements in Analysis and Design*, **44**, pp. 875-888 (2008).
19. Reddy, R. M. and Rao, B. N., "Continuum Shape Sensitivity Analysis of Mixed-Mode Fracture Using Fractal Finite Element Method," *Engineering Fracture Mechanics*, **75**, pp. 2860-2906 (2008).
20. Rao, B. N. and Reddy, R. M., "Fractal Finite Element Method Based Shape Sensitivity Analysis of Multiple Crack System," *Engineering Fracture Mechanics*, **76**, pp. 1636-1657 (2009).
21. Dong, C. Y., Lo, S. H. and Cheung, Y. K., "Numerical Solution for Elastic Half-Plane Inclusion Problems by Different Integral Equation Approaches," *Engineering Analysis with Boundary Elements*, **28**, pp. 123-140 (2004).
22. Chen, J. T., Shen, W. C. and Chen, P. Y., "Analysis of Circular Torsion Bar with Circular Holes Using Null-Field Approach," *CMES: Computer Modeling in Engineering & Sciences*, **12**, pp. 109-119 (2006).
23. Chen, J. T., Hsiao, C. C. and Leu, S. Y., "Null-field Integral Equation Approach for Plate Problems with Circular Boundaries," *ASME Journal of Applied Mechanics*, **73**, pp. 679-693 (2006).
24. Shiah, Y. C. and Chong, J. Y., "Boundary Element Analysis of Interior Thermoelastic Stresses in Three-Dimensional Generally Anisotropic Bodies,"

https://doi.org/10.1017/jmech.2018.45 Published online by Cambridge University Press

Journal of Mechanics, **32**, pp. 725-735 (2016).

25. Shiah, Y. C. and Chang, L. D., "Boundary Element Calculation of Near-Boundary Solutions in 3D Generally Anisotropic Solids by the Self-Regularization Scheme," *Journal of Mechanics*, **33**, pp. 813-820 (2017).
26. Liu, D. S. and Chiou, D. Y., "A Coupled IEM/FEM Approach for Solving the Elastic Problems with Multiple Cracks," *International Journal of Solids and Structures*, **40**, pp. 1973-1993 (2003).
27. Liu, D. S. and Chiou, D. Y., "3D IEM Formulation with an IEM/FEM Coupling Scheme for Solving Elastostatic Problems," *Advances in Engineering Software*, **34**, pp. 309-320 (2003).
28. Liu, D. S. and Chiou, D. Y., "Modeling of Inclusion with Interphases in Heterogeneous Material Using the Infinite Element Method," *Computational Materials Science*, **31**, pp. 405-420 (2004).
29. Liu, D. S., Chen, C. Y. and Chiou, D. Y., "3D Modeling of a Composite Material Reinforced with Multiple Thickly Coated Particles Using the Infinite Element Method," *CMES: Computer Modeling in Engineering & Sciences*, **9**, pp. 179-191 (2005).
30. Liu, D. S., Zhuang, Z. W. and Chung, C. L., "Modeling of Moisture Diffusion in Heterogeneous Epoxy Resin Containing Multiple Randomly Distributed Particles Using Hybrid Moisture Element Method," *CMC: Computers Materials & Continua*, **13**, pp. 89-113 (2009).
31. Liu, D. S., Zhuang, Z. W., Lyu, S. R., Chung, C. L. and Lin, P. C., "Modeling of Moisture Diffusion in Permeable Fiber-Reinforced Polymer Composites Using Heterogeneous Hybrid Moisture Element Method," *CMC: Computers Materials & Continua*, **26**, pp. 111-136 (2011).
32. Liu, D. S., Fong, Z. H., Lin, I. H. and Zhuang, Z. W., "Modeling of Moisture Diffusion in Permeable Particle-Reinforced Epoxy Resins Using Three-Dimensional Heterogeneous Hybrid Moisture Element Method," *CMES: Computer Modeling in Engineering & Sciences*, **93**, pp. 441-468 (2013).
33. Liu, D. S., Tu, C. Y. and Chung, C. L., "Eigenvalue Analysis of Mems Components with Multi-Defect Using Infinite Element Method Algorithm," *CMC: Computers Materials & Continua*, **28**, pp. 97-120 (2012).
34. Liu, D. S., Tu, C. Y. and Chung, C. L., "Coupled PIEM/FEM Algorithm Based on Mindlin-Reissner Plate Theory for Bending Analysis of Plates with Through-Thickness Hole," *CMES: Computer Modeling in Engineering & Sciences*, **92**, pp. 573-594 (2013).
35. Liu, D. S. and Lin, Y. H., "Vibration Analysis of the Multiple-Hole Membrane by Using the Coupled DIEM-FE Scheme," *Journal of Mechanics*, **32**, pp. 163-173 (2016).
36. Jain, J., Li, H., Cauley, S., Koh, C. K. and Balakrishnan, V., "Numerically Stable Algorithms for Inversion of Block Tridiagonal and Banded Matrices," *Purdue University TR ECE*, pp. 357 (2007).

(Manuscript received May 16, 2018,
accepted for publication July 31, 2018.)

https://doi.org/10.1017/jmech.2018.45 Published online by Cambridge University Press